Nonreciprocal Isolation and Wavelength Conversion via a Spatiotemporally Engineered Cascaded Cavity

Xingping Zhou,[1,2,§] Samit Kumar Gupta,[1,3,§] Xueyi Zhu,[1,3] Guangxu Su,[1,2] Peng Zhan,[1,2,5,*] Yongmin Liu,[4,†] Zhuo Chen,[1,2,5] Minghui Lu,[1,3,5] and Zhenlin Wang[1,2,5,‡]

[1] *National Laboratory of Solid State Microstructures, Nanjing University, Nanjing 210093, China*

[2] *School of Physics, Nanjing University, Nanjing 210093, China*

[3] *College of Engineering and Applied Sciences, Nanjing University, Nanjing 210093, China*

[4] *Department of Mechanical and Industrial Engineering and Department of Electrical and Computer Engineering, Northeastern University, Boston, Massachusetts 02115, USA*

[5] *Collaborative Innovation Center of Advanced Microstructures, Nanjing University, Nanjing 210093, China*

(Received 15 March 2019; revised manuscript received 22 February 2020; accepted 20 March 2020; published 14 April 2020)

The principle of reciprocity underpins one of the fundamental effects in optics that signifies symmetric transmission with respect to the interchange of the source and observation points. Breaking reciprocity, however, enables additional functionalities and greatly enriches the applications of photonics in terms of nonreciprocal devices. Here, a realistic nanoscale cascaded-cavity system that envisages nonreciprocal optical isolation and efficient wavelength conversion based on spatiotemporally modulated index of refraction are proposed and numerically demonstrated. The on-chip, linear, magnetic-free nonreciprocal isolation and dynamically controllable wavelength conversion can be a promising candidate for silicon nanophotonic and optoelectronic devices.

DOI: 10.1103/PhysRevApplied.13.044037

I. INTRODUCTION

In classical electromagnetism, the principle of Lorentz reciprocity states that the response of a transmission channel is symmetric when source and observation points are interchanged. It implies the symmetry in Green's functions, and the identical reception and radiation property of antennas [1–3]. Breaking Lorentz reciprocity enables optical nanostructures to be used for intriguing functionalities such as optical isolation, which plays significant roles in efficient design of integrated optical systems via laser feedback protection, alleviating multipath interference not achievable in reciprocal structures [4,5].

A couple of distinctive yet conventional approaches exist toward creating nonreciprocity to achieve optical isolation. Applying an external magnetic field, which can lead to the asymmetric permittivity tensor of magneto-optical materials, is the most common way to break the reciprocity between forward and backward propagating modes [6–10]. However, magneto-optical materials are typically very lossy at optical frequencies, and it is challenging to integrate them on chip-scale devices with low cost and in a CMOS compatible manner. Recently, due to the great demand for nonreciprocal photon transport in miniaturized and chip-compatible systems, alternative strategies for nonmagnetic optical isolation have been proposed. For instance, using optical nonlinearity, Lorentz reciprocity could be broken due to the dependence of the dielectric function on the electric field strength, but these are typically limited to specific operating conditions and strong input signals [5]. In addition, we can achieve nonreciprocity by biasing with other quantities that break time-reversal symmetry, including direct electric current [11,12].

More recently, the dynamic temporal modulation of refractive index has been widely explored to break the Lorentz reciprocity [12–18], which promises a new route towards magnetic-free and on-chip nonreciprocal components, like optical isolators and circulators. This dynamic time modulation can be incorporated in several ways, imparting a synthetic linear or angular momentum to a structure without moving its constituting parts. As a typical example, in a spatiotemporally modulated waveguide [13], a shift of energy and momentum can be provided by the space-time modulation to enable a transition between two photonic modes propagating along one direction. However, no transition occurs in the opposite direction due to the mismatch of energy and momentum. Therefore, transmission through a spatiotemporally modulated waveguide is nonreciprocal, and time-reversal symmetry is broken

*zhanpeng@nju.edu.cn
†y.liu@northeastern.edu
‡zlwang@nju.edu.cn
§These authors contributed equally to this work.

 © 2020 American Physical Society

by the directionality of the modulation. Another form of time modulation to induce nonreciprocity is based on synthetic angular momentum without using magnetic materials. Giant nonreciprocity has been observed by imparting angular momentum to an azimuthally symmetric cavity [19–22]. Moreover, optomechanics can also provide yet another useful way to efficiently induce temporal modulations via mechanical resonances that are excited and strongly coupled to optical signals [23–27].

On the other side, nonreciprocal wavelength conversion poses an interesting aspect of optical systems where on-demand manipulation of optical signals could be suggestive of immense practical importance in optical communication [28]. For example, it can be employed for various optical engineering technologies such as information processing in wavelength-demultiplexing (WDM) communication systems [29,30]. It has been observed that it is possible to realize efficient wavelength conversion in photonic systems [31–37] via some dynamic processes. Typically, it necessitates the use of highly nonlinear materials, which, however, could be a rather difficult process in terms of on-chip integration and efficiency. In recent decades, there have been significant advancements in the manipulation of light using photonic nanocavities [38–41], which are key components in trapping and storing photons. By spatiotemporal modulation, a nonreciprocal trapping of light has been proposed to demonstrate the possibility of unidirectional exponential accumulation of photons traveling in only one direction with a controllable shifting frequency [42]. In this paper, we demonstrate nonreciprocal optical isolation and wavelength conversion based on dynamic refractive index modulation in a cascaded-cavity system. Such an on-chip, linear, magnetic-free system of cascaded nanocavities provides another efficient means toward nonreciprocal isolation on a feasible silicon nanophotonic platform, which promises a wealth of integrated photonic and optical communication applications. In addition, the dynamically controllable wavelength shift is scaled with the number of cavities, which breaks the wavelength conversion limit imposed by the limitation in index change. Moreover, it could provide a useful setting to investigate and manipulate transport and trapping of photons via effective tuning and design of such cascaded nanocavities.

II. RESULTS AND DISCUSSION

To elaborate on the idea, we consider the lock for water navigation shown in Fig. 1(a). The raising or lowering of the water level is analogous to the process of employing dynamic tuning. The working principle of a navigation lock thus provides an intuitive picture of the nonreciprocal isolation and wavelength conversion of the cascaded-cavity system. Mathematically, the spatiotemporal refractive index distribution in Fig. 1(b) can be described by

$$n(x,t) = n_0 + \Delta n \times u(t-t_1) \times [u(x-x_1) - u(x-x_2)] + \Delta n \times u(t-t_2) \times [u(x-x_3) - u(x-x_4)]. \quad (1)$$

Here, $u(x)$ stands for the step function. t_1 and t_2 refer to the instants of time of introducing dynamic tuning in cavities II and III, and the intervals $[x_1, x_2]$ and $[x_3, x_4]$ correspond to the defect areas of those cavities.

In order to implement the above-mentioned idea, first, we need to consider a viable platform in which the energy can be transferred between different locations. Embedding artificial defects as cavities in periodic structure is an important avenue to manipulate localization and produce local resonant modes. We take advantage of Rabi oscillation in two such cavities to transfer energy [31]. For the sake of simplicity, two one-dimensional (1D) photonic crystal cavities are designed to generate Rabi oscillation. Moreover, the Rabi oscillation state can be stopped on demand by dynamic control of either of the two nanocavities, freezing the photon state [31,32,43]. The 1D photonic crystal (PtC) cavity can be fabricated by the thin-film deposition process, which can adjust the thickness of different layers of the PtCs conveniently. Due to periodicity and linearity of the resonance wavelength varying with length of the defect layer in the bandgap [44], the length of

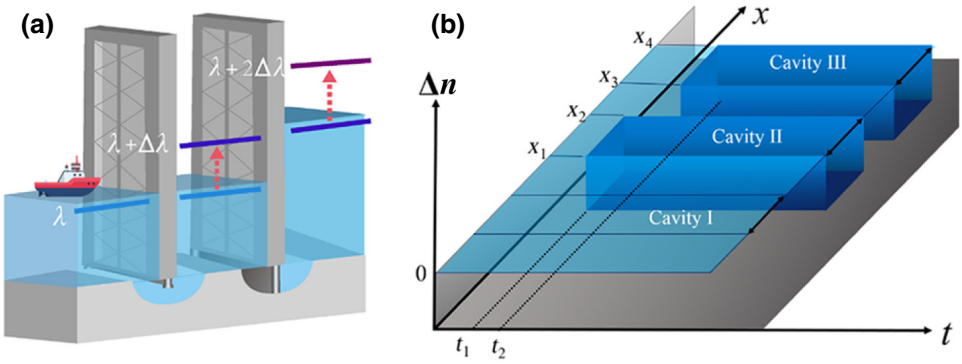

FIG. 1. (a) Schematic of a lock for water navigation. Energy-level diagram of the cascaded-cavity system is shown to depict the analogy between these two seemingly different systems. (b) Schematic of spatiotemporal modulation of refractive index in cascaded photonic cavities.

defect layer can be fine tuned to meet the requirements in experiment. Time-varying materials are used to simulate the control process (like an electrical control process) [45]. The finite-difference time-domain (FDTD) method can be conveniently used as it can easily take into account the variation of material parameters in time. Second, we design a cascaded-cavity system so that the energy can be transmitted in each of the cavities in turn. The resonance wavelength of the second cavity (defined as cavity B) after applying the dynamic modulation is the same as prior to applying the dynamic modulation of the third cavity (defined as cavity C), so that energy can be transferred (from cavity B to cavity C). To satisfy this condition, we consider a proper choice of the thickness of the defect layer (since the resonant wavelength of the cavity varies with the thickness of the defect layer). For simplicity, we choose three cavities to form the cascaded-cavity system. This way the nanoscale cascaded-cavity system is designed in which we demonstrate optical isolation and wavelength conversion by means of dynamic time modulation.

Prior to the three-cavity system, we first consider a two-cavity system as shown in Fig. 2(a), in which the system consists of two 1D photonic crystal nanocavities separated by a distance. As can be seen, the two cavities effectively form a Fabry-Perot (FP) cavity in the middle. The two resonant cavities can be coupled at resonance through this FP cavity as a medium to achieve strong remote coupling [43]. The Q factor of the resonance mode of the cavity can simply be increased by adding the number of layers so that its Q factor is greater than that of the FP cavity mode to satisfy the long-range strong-coupling condition [31]. In order to increase the Q factor of the whole system, we add three more periods to the outside of the two resonant cavities. The transmission spectrum of this two-cavity system is calculated through the FDTD algorithm as can be seen on the left panel of Fig. 2(b). Two resonant peaks around 554.2 nm are observed around the resonance peak of the single cavity as shown in Fig. 2(b). The band diagram (performed by a free and open-source software package MPB [46]) of this two-cavity system, which composed of one-dimensional strip superlattices, has been depicted on the right panel of Fig. 2(b). The corresponding modes of these two peaks are the Rabi splitting modes, which are shown as the blue and pink solid lines in the photonic band diagram. On the other side, the peak around 553.9 nm corresponding to the FP-cavity mode is shown in the green solid line in the band diagram. The locations of the photonic bands perfectly correspond to the peak positions in the transmission spectrum. The electric field distributions of the two Rabi splitting modes are depicted in Fig. 2(c), which clearly show symmetric and antisymmetric field profile, respectively. In Fig. 2(d), the transmission through the coupled system is plotted as a function of distance between the two cavities on an expanded wavelength scale. It is evident

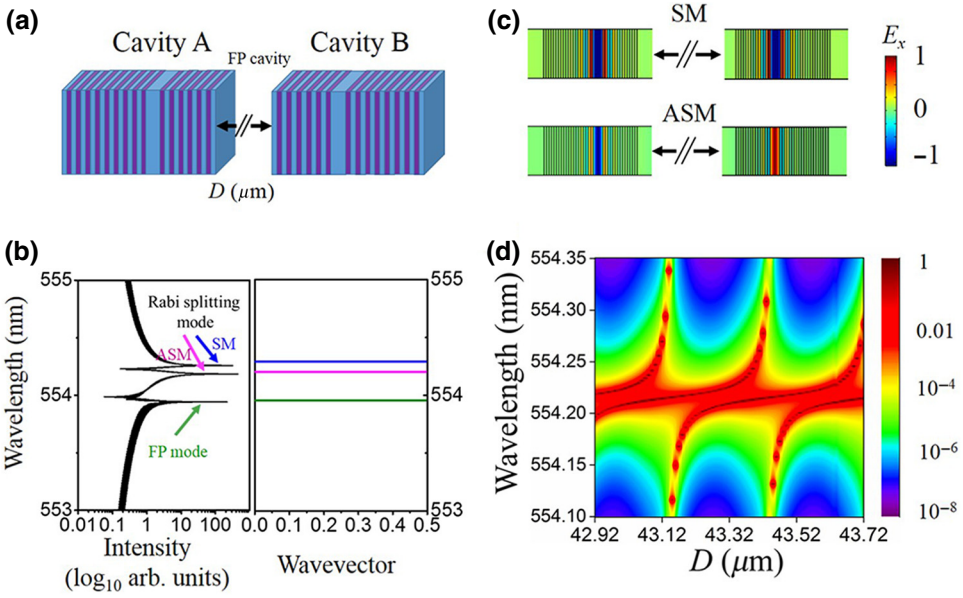

FIG. 2. (a) Conceptual schematic of the proposed structure, consisting of two 1D photonic crystal cavities. Periodically stacked 50-nm-thick dielectric layers (colored blue) with a refractive index of 1.4- and 50-nm-thick dielectric layers (colored purple) of 3.4 are used to form the 1D photonic crystal. The thickness of defect layer is set as 200 nm, and the distance between the two cavities (D) is 42.8 μm (much larger than resonant wavelength of the single cavity). (b) (Left panel) The transmission spectrum of this dual-cavity system and the corresponding photonic band diagram (right panel) for $D = 42.8$ μm. (c) Electric fields of the symmetric mode (SM) and the antisymmetric mode (ASM). (d) Calculated transmission spectra of the system dependent on the distance between two cavities (D).

that there are two transmission peaks for a fixed separation distance. The anticrossing behavior of the two peaks is characteristic of strong-coupling phenomena.

We investigate the time-domain behavior of the Rabi peaks, with cavity A being excited by a single pulse (center wavelength, around 554 nm; wavelength width, about 1 nm) that covers both Rabi splitting modes. As shown in Fig. 3(a), the black and red solid lines denote the amplitudes in the cavities A and B, respectively, at different times. When signal light (centered at 554 nm with 1 nm of pulse width) is incident from the resonant cavity A, the energy in this cavity increases until the instant of time when the energy is transferred to the cavity B. After this, energy is exchanged between both of the cavities. Clearly, the amplitude of Rabi oscillation decreases, which is due to the radiation loss of energy of the whole system. Figure 3(b) shows the optical field energy distributions at different instants of time. Notably it can be seen that while at 60.6 ps, the energy is concentrated in the resonant cavity A, at 66.9 ps (75.6 ps), the energy is partially (completely) transferred to cavity B. Then we demonstrate dynamic control over these coupling states to explore the energy evolution in time domain. We use a step function to simulate temporal modulation on refractive index of the defect layer in the cavity. First, we excite cavity A by a single pulse that leads to energy exchange between the two cavities. Then, the control pulse is irradiated onto cavity B at around 90 ps (indicated by the dashed gray line). For simplicity, we assume that the control pulse only induces an increase of the refractive index ($\Delta n/n = 1\%$) of the defect layer in cavity B. As shown in Fig. 3(c), since the resonant wavelength of the resonant cavity B changes at this instant of time, it ceases the Rabi oscillation. The resonant wavelength of cavity B shifts about 6 nm as a result of this dynamic control, so that photons in cavity A no longer couple to cavity B. Ideally, the photon population is frozen in the state at the moment of dynamic control. However, due to the radiation loss, the field amplitude (or photon population) in cavity B gradually decays. In Fig. 3(d), at around 100 ps, the refractive index of the cavity B defect layer is changed with dynamic control, and after 175 ps the control is stopped (the refractive index of the defect layer returns to the initial value). We can observe three distinctive regions in the spectra, showing that the strong coupling and Rabi oscillations between the cavities can be controlled via dynamic refractive-index tuning.

The transmission spectrum can be obtained by a wavelength meter in experiment. The control pulse can be split from the signal pulse for the dynamic tuning process. It should be passed through a delay device before acting on the sample. The phase delay can be realized by optical gratings, or photonic crystal waveguides, which possess slow light characteristics. It is not limited to optical settings. The

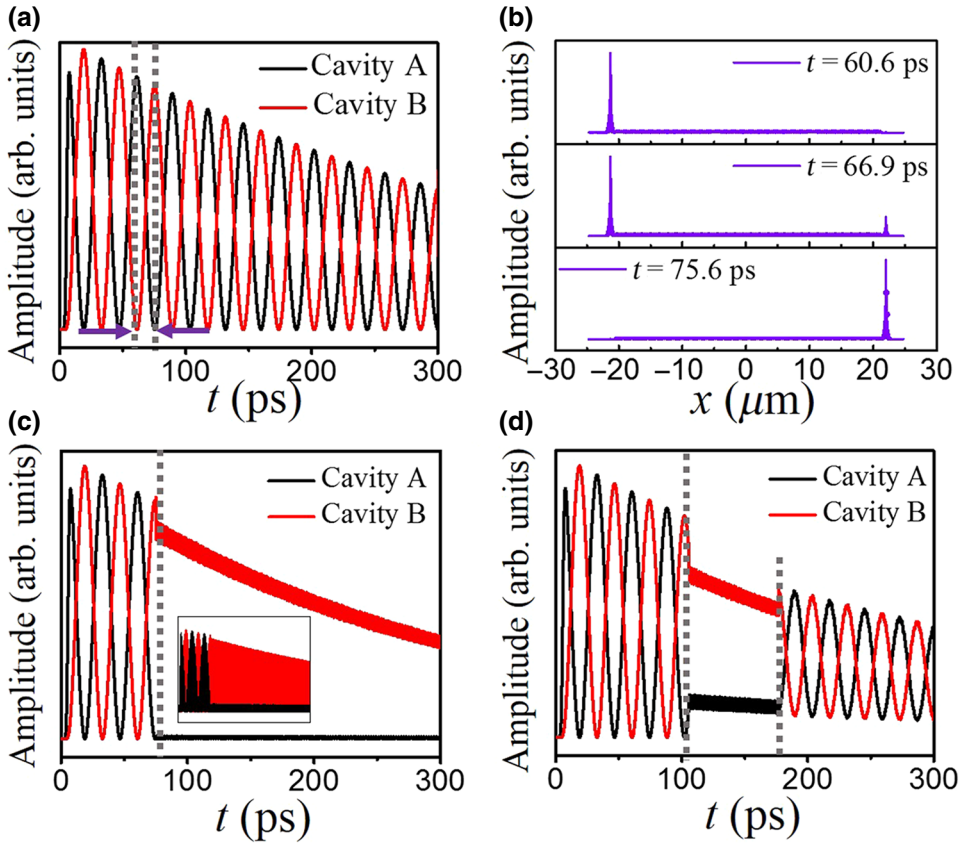

FIG. 3. (a) Evolution of the amplitudes observed in the two-coupled cavities. The gray dashed frame refers to a period of oscillation, which is about 60.6–75.6 ps. (b) Amplitude distribution in the system at different instants of time. The positions of cavity A and B are at about -22 μm and 22 μm. (c) Evolution of the amplitudes observed in each of the cavities, while the refractive index of cavity B can be modulated by an electrical control. The inset shows the data before removing the high-frequency component. (d) Evolution of the amplitudes where the control pulse is irradiated into cavity B and then the control pulse stops.

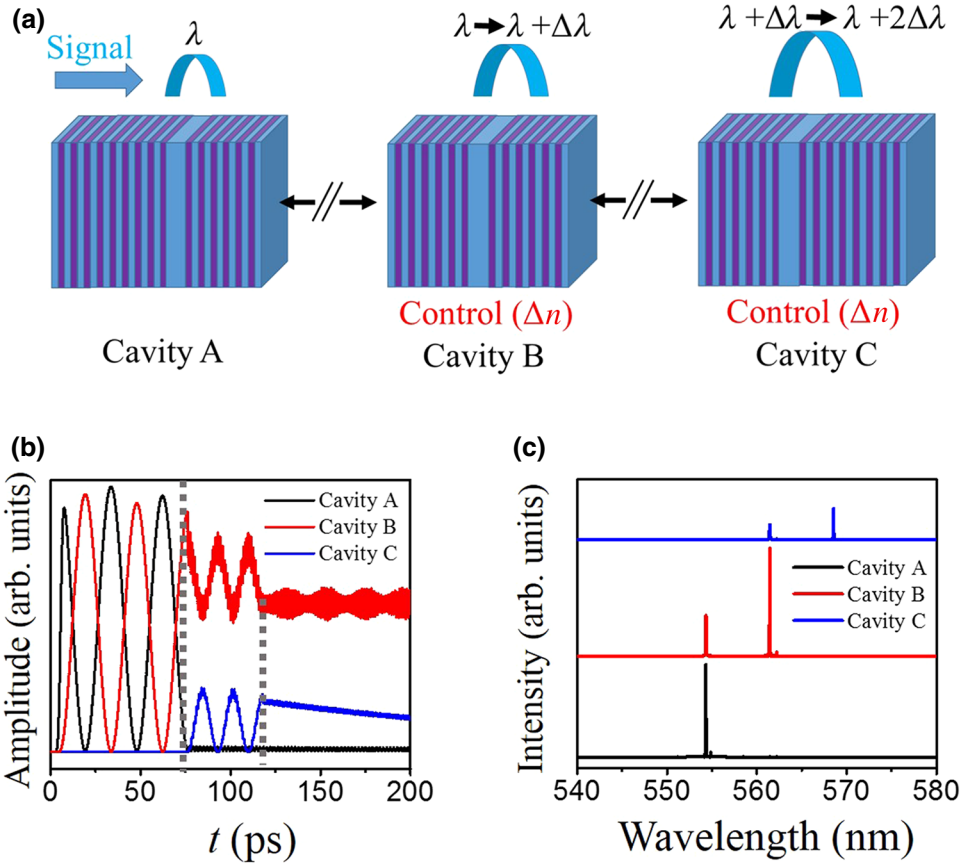

FIG. 4. (a) Schematic of the cascaded-cavity system, consisting of three one-dimensional photonic crystal cavities. The distance between adjacent cavities is 42.8 μm. Similar to the previous one, cavity A and B have the same defect layer thickness and resonant wavelength, so that energy can be directly transferred between these two cavities. (b) Amplitude evolution observed in each cavity where the control pulse is irradiated into cavity B, and C in sequence. (c) Spectrum of the light in cavity A, B, and C, respectively.

electro-optic tuning with a sort of delay circuit can also be considered to dynamically tune the sample.

We now consider a three-cavity system as shown in Fig. 4(a). Pump light is used to irradiate cavity B and the refractive index of the defect layer in it is increased ($\Delta n/n = 1\%$), which leads to dynamical control and wavelength conversion. At this point, due to the different resonance wavelengths of cavities A and B, energy ceases to exchange between them. We design the resonant cavity C such that the length of the defect layer is 205 nm, which makes its resonant wavelength ($\lambda = 561$ nm) to be the same as that of cavity B after dynamic tuning. Consequently, cavities B and C satisfy the Rabi oscillation condition, resulting in energy transfer between the two cavities. We use the FDTD algorithm again to calculate the time-dependent amplitudes in the three cavities. Figure 4(b) depicts the amplitudes in cavities A, B, and C represented by black, red, and blue solid lines, respectively. By dynamic refractive-index tuning of the cavities in sequence (indicated by the two gray dashed lines), energy is transferred from resonator A to resonator C. When the energy in the system decays to zero, the Fourier transform of the energy in each cavity is taken to calculate the frequency-domain spectrum. One can see that there is only one resonant wavelength of 554 nm in cavity A as opposed to the two resonance wavelengths of 554 and 561 nm in cavity B, the latter being the new resonance wavelength induced via dynamic tuning. Similarly, one can find two resonance wavelengths of 561 and 568 nm in cavity C. We know that optical wavelength conversion can be induced by dynamic tuning of refractive index [33]. However, the wavelength shift $\Delta\lambda$ in this process is strongly dependent on the index change $\Delta n/n$ such that $\Delta\lambda/\lambda \approx \Delta n/n$. The cascaded-cavity system we propose here can overcome this drawback by transferring energy between different cavities, which essentially results in larger interaction length to enhance the wavelength shift. In the three-cavity system, we obtain a wavelength conversion of 14 nm, breaking the wavelength conversion limit imposed by the refractive-index change limitation. Notably, there is some energy in cavity B, which cannot be transferred to cavity C. This is due to the imperfect Rabi oscillation condition between cavity B and C. The conversion efficiency (γ) can be roughly defined as $\gamma = W_C/(W_A + W_B + W_C)$. Here, W represents the energy in each corresponding photonic cavity, which is positive correlation with I^2 (I is defined as the value of the envelope of $|E|$). Therefore, the conversion efficiency is assessed at $\gamma = I_C{}^2/(I_A{}^2 + I_B{}^2 + I_C{}^2) \approx 6.25\%$.

In order to demonstrate the nonreciprocal optical process accompanied by wavelength conversion through a spatiotemporal dynamical modulation, we perform

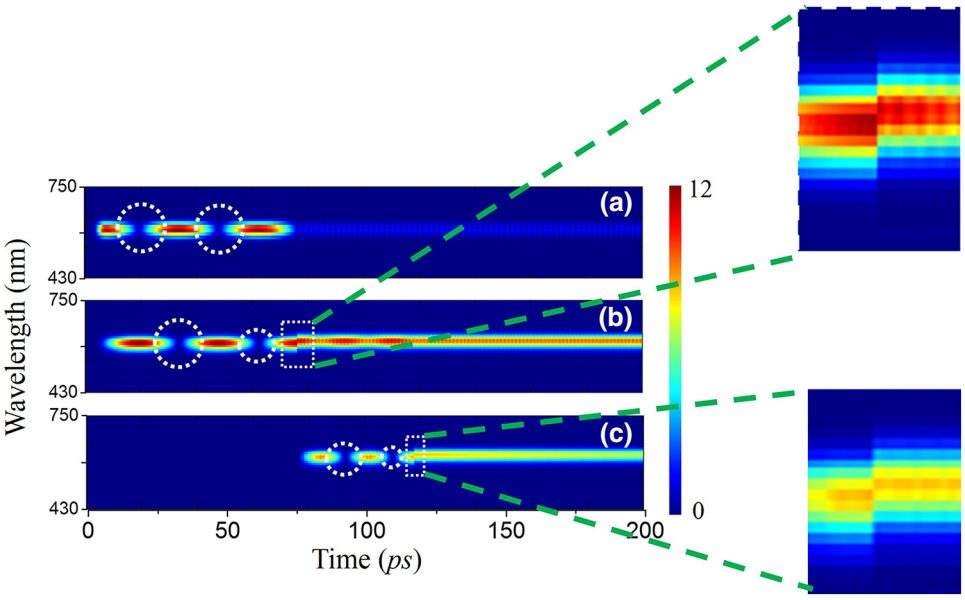

FIG. 5. Wavelet transform of signals in cavity A, B, and C, respectively.

systematic numerical calculation to investigate optical energy transfer in the proposed cascaded cavity in time and frequency domain. Notably, although this dynamic tuning should be performed in time domain, the conventional mathematical method based on Fourier transform leads to the loss of time information while performing the information processing from frequency to time domain. This essentially means that there are some limitations to the nonstationary process by Fourier transform. In such a situation, one can find that the wavelet transform is an effective mathematical tool for local transformation in both time and frequency domains. By the method of multiscale analysis carried out on functions or signals via scaling and shifting, it provides a useful means for solutions toward many potential issues beyond the reach of Fourier transform [47,48].

Generally, the wavelet transform process can be described as

$$X(a,\tau) = \frac{1}{\sqrt{a}} \int_{-\infty}^{\infty} f(t)\psi\left(\frac{t-\tau}{a}\right) dt. \tag{2}$$

Unlike Fourier transform, wavelet transform has two variables: the scale and shift. The scale "a" stands for the scaling of the wavelet function, corresponding to the frequency, and the shift "τ" is related to the time domain of the wavelet function. In this way, we can get a time-frequency spectrum through wavelet transform, while the Fourier transform can only get a frequency spectrum. To get the smooth continuous wavelet amplitude, we choose the nonorthogonal wavelet function, Morlet wavelet [48], which is formulated by

$$\psi_0(t) = \pi^{-1/4} e^{i\omega_0 t} e^{-t^2/2}, \tag{3}$$

where t is time and ω_0 is dimensionless frequency.

Then we can perform the wavelet transform to analysis the signals in each cavities. It can be seen from the Fig. 5(a) that before the action of dynamic tuning on cavity B at 76 ps, there is no energy in cavity A at 19.5 and 48 ps because of the mutual transfer of energy in cavity A and B, so there is a disconnection in the wavelet time-frequency diagram indicated by white dashed circles. After 76 ps, the Rabi oscillation condition between cavity A and cavity B has been destroyed, and the energy is localized in cavity A without exchanging, so the time-frequency diagram is continuous. Note that here we do not perform the dynamic tuning on cavity A, so the wavelength of the light in cavity A keep unchanged.

Next, we perform wavelet analysis on cavity B. It can be seen from Fig. 5(b), similar to the situation in cavity A, because of the energy transfer between cavity A and B, the energy in cavity B is close to zero at 34 and 62.5 ps, resulting in discontinuity in the time-frequency image of wavelet transform indicated by white dashed circles. Unlike the situation in cavity A, the wavelength of cavity B changes due to the dynamic tuning at 76 ps. From the white dashed frame in the wavelet time-frequency diagram, we can see that the frequency shifts to the low frequency (long wavelength), indicating the realization of wavelength conversion. Between 76 and 119 ps, due to the energy oscillation between cavity B and C, we can see that the intensity has changed periodically from the wavelet time-domain diagram. 119 ps later, the intensity remains stable for the stop of energy exchange, i.e., only one frequency of light wave exists in cavity B, because of the broken of the Rabi oscillation condition.

At last, the signal in cavity C is analyzed by wavelet transform. From the wavelet time-frequency diagram in Fig. 5(c), it can be seen that there is no energy in cavity C before time 76 ps. Between 76 and 119 ps, cavity B and

C satisfy the Rabi oscillation condition and energy transfer occurs due to the dynamic tuning on cavity B. At 93 and 110 ps, the intensity of the wavelet time-frequency diagram is near to zero (indicated by white dashed circles), which is due to the zero energy in cavity C at those instant times. 119 ps later, due to dynamic tuning on cavity C, wavelength conversion occurs (indicated by a white dashed box), and energy transfer with cavity B stops. The intensity of the wavelet time-frequency diagram tends to be stable.

Our proposed system can be extended to multiple-cavity system with a larger wavelength shift. The wavelength shift can approximately be given by $\Delta\lambda/\lambda \approx (N-1)(\Delta n/n)$, where N is the number of cavities. In addition, we also find analytic forms to illustrate the wavelength conversion of the cascaded system by signals and systems theory [49], which are given within the Supplemental Material [50].

Different orders of modes can be generated via spatial symmetry breaking that can induce effects similar to nonreciprocity. But in fact, those cases can be very different from nonreciprocal behaviors since here all possible states for backward propagation are not blocked or diverted [4]. As single-mode cavities are used in our system, which can be indicated by the photonic band diagram of the whole system as shown in Fig. 2(c), no higher-order modes can be excited. We further study the nonreciprocal propagation of light through the three-cavity system. We only change the direction of the incident pulse, while other parameters are fixed in the simulation. To have a quantitative idea about the nonreciprocity of the device, the amplitude at the outgoing port of the system is recorded when the system enters a stable state. The asymmetrical response of light waves in forward and backward directions of the system reveals the strong nonreciprocal isolation when a light source enters from opposite directions as is evident from Fig. 6. The isolation ratio can be defined as $-10\log_{10}[(I_{\text{backward}})/(I_{\text{forward}})]$ (I stands for the value of the envelope of the $|E|$). The time-domain isolation ratio shown in Fig. 6 clearly gives a quantitative measure of strong nonreciprocity (around -45 dB). Our design can achieve a nonreciprocal defect mode in which the photons can propagate in one direction and become localized, while in the opposite direction, photons with the same frequency get reflected. Unlike previous counterparts, our proposed device has nonreciprocity effects only for a period of time, unless the device is reset. We can redesign and rescale the whole system (since Maxwell's equations are scale invariant) to obtain nonreciprocal isolation over other frequency ranges. It is worth noting here that, in our calculation model, we do not consider the material loss. While the material loss introduces additional energy dissipation in the system, nonreciprocal phenomena still persist. In addition, we can extend the system to a larger number of 1D chains of cavities to obtain optical isolation and larger wavelength conversion (see Fig. S2 within the Supplemental Material [50]).

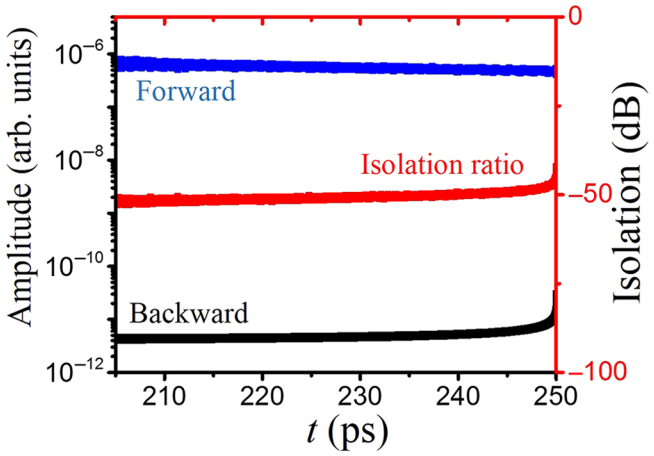

FIG. 6. Optical isolation behavior of the three-cavity system in time domain. Blue and black solid lines correspond to the calculated amplitudes of the system for forward and backward directions. The red solid line corresponds to the isolation ratio.

III. CONCLUSION

In summary, a practical physical system has been designed to achieve wavelength conversion and nonreciprocal optical isolation in a cascaded-cavity system by means of dynamic refractive-index modulation. Dynamic refractive-index tuning, which plays a significant role in their practical realizations has provided a useful means to predict and realize some of the intriguing physical effects in various practical settings [11]. We show that the chip-compatible, compact, and linear system of cascaded nanocavities provides another useful and efficient nonmagnetic platform to achieve strong nonreciprocal isolation. In addition, it gives rise to dynamically controllable nonreciprocal wavelength conversion that breaks the constraint imposed by limitation in index change. Besides, the cascaded nanocavities with dynamic tuning exemplifies transfer and trapping of photons via judicious tuning and design of the system. Moreover, it can also provide a versatile platform to investigate and manipulate photon transport and localization [42], which is likely to enhance its application prospects. This work thus provides a useful avenue toward effective design of nonreciprocal optical components based on dynamic refractive-index tuning, for tailoring photon transport in optical communication and nanophotonic devices.

ACKNOWLEDGMENTS

This work is supported by the national Key R&D Program of China (Grants No. 2017YFA0303702 and

No. 2018YFA0306202), and National Natural Science Foundation of China (Grants No. 11834007, No. 11674166, No. 11774162, No.11625418, No. 51732006, and No. 11621091).

[1] R. J. Potton, Reciprocity in optics. Rep. Prog. Phys. **67**, 717 (2004).
[2] G. A. Kriegsmann, The flanged waveguide antenna: Discrete reciprocity and conservation. Wave Motion **29**, 81 (1999).
[3] M. Born, and E. Wolf, *Principles of Optics*, 7th ed. (Cambridge University Press, Cambridge, England, 1997).
[4] D. Jalas, A. Petrov, M. Eich, W. Freude, S. Fan, Z. Yu, R. Baets, M. Popović, A. Melloni, J. D. Joannopoulos, M. Vanwolleghem, C. R. Doerr, and H. Renner, What is – and what is not—and optical isolator, Nat. Photon. **7**, 579 (2013).
[5] Y. Shi, Z. Yu, and S. Fan, Limitations of nonlinear optical isolators due to dynamic reciprocity. Nat. Photon. **9**, 388 (2018).
[6] Z. Wang, Y. Chong, J. D. Joannopoulos, and M. Soljačić, Observation of unidirectional backscattering-immune topological electromagnetic states. Nature **461**, 772 (2009).
[7] Y. Poo, R. X. Wu, Z. Lin, Y. Yang, and C. T. Chan, Experimental Realization of Self-Guiding Unidirectional Electromagnetic Edge States. Phys. Rev. Lett. **106**, 093903 (2011).
[8] K. Fang, Z. Yu, and S. Fan, Microscopic theory of photonic one-way edge mode. Phys. Rev. B **84**, 075477 (2011).
[9] Y. Hadad, A. R. Davoyan, N. Engheta, and B. Z. Steinberg, Extreme and quantized magneto-optics with graphene meta-atoms and metasurfaces. ACS Photon. **1**, 1068 (2014).
[10] M. Tien, T. Mizumoto, P. Pintus, H. Kromer, and J. Bowers, Silicon ring isolators with bonded nonreciprocal magneto-optic garnets. Opt. Express **19**, 11740 (2011).
[11] H. B. G. Casimir, On Onsager's principle of microscopic reversibility. Rev. Mod. Phys. **17**, 343 (1945).
[12] D. L. Sounas, and A. Alù, Non-reciprocal photonics based on time modulation. Nat. Photon. **11**, 774 (2017).
[13] Z. Yu, and S. Fan, Complete optical isolation created by indirect interband photonic transitions. Nat. Photon. **3**, 91 (2009).
[14] K. Fang, Z. Yu, and S. Fan, Realizing effective magnetic field for photons by controlling the phase of dynamic modulation. Nat. Photon. **6**, 782 (2012).
[15] Y. Hadad, D. Sounas, and A. Alù, Space-time gradient metasurfaces. Phys. Rev. B **92**, 100304 (2015).
[16] A. Shaltout, A. Kildishev, and V. Shalaev, Time-varying metasurfaces and Lorentz non-reciprocity. Opt. Mater. Express **5**, 2459 (2015).
[17] D. W. Wang, H. T. Zhou, M. J. Guo, J. X. Zhang, J. Evers, and S. Y. Zhu, Optical Diode Made From a Moving Photonic Crystal. Phys. Rev. Lett. **110**, 093901 (2013).
[18] Z. Yu, and S. Fan, Optical isolation based on nonreciprocal phase shift induced by interband photonic transitions. Appl. Phys. Lett. **94**, 171116 (2009).
[19] D. L. Sounas, C. Caloz, and A. Alù, Giant non-reciprocity at the subwavelength scale using angular momentum-biased metamaterials. Nat. Commun. **4**, 2407 (2013).
[20] N. A. Estep, D. L. Sounas, J. Soric, and A. Alù, Magnetic-free non-reciprocity and isolation based on parametrically modulated coupled-resonator loops. Nat. Phys. **10**, 923 (2014).
[21] D. L. Sounas, and A. Alù, Tunable orbital angular momentum radiation from angular-momentum-biased microcavities. ACS Photon. **1**, 198 (2014).
[22] N. A. Estep, D. L. Sounas, and A. Alù, Magnetless microwave circulators based on spatiotemporally modulated rings of coupled resonators. IEEE Trans. Microwave Theory Tech. **64**, 502 (2016).
[23] A. Metelmann, and A. Clerk, Nonreciprocal Photon Transmission and Amplification via Reservoir Engineering. Phys. Rev. X. **5**, 021025 (2015).
[24] K. Fang, J. Luo, A. Metelmann, M. H. Matheny, F. Marquardt, A. A. Clerk, and O. Painter, Generalized non-reciprocity in an optomechanical circuit via synthetic magnetism and reservoir engineering. Nat. Phys. **13**, 465 (2017).
[25] Z. Shen, Y.-L. Zhang, Y. Chen, C.-L. Zou, Y.-F. Xiao, X.-B. Zou, F.-W. Sun, G.-C. Guo, and C.-H. Dong, Experimental realization of optomechanically induced non-reciprocity. Nat. Photon. **10**, 657 (2016).
[26] F. Ruesink, M. A. Miri, A. Alù, and E. Verhagen, Nonreciprocity and magnetic-free isolation based on optomechanical interactions. Nat. Commun. **7**, 13662 (2016).
[27] M. A. Miri, F. Ruesink, E. Verhagen, and A. Alù, Optical Nonreciprocity Based on Optomechanical Coupling. Phys. Rev. Appl. **7**, 064014 (2017).
[28] A. Kamal, A. Roy, J. Clarke, and M. H. Devoret, Asymmetric Frequency Conversion in Nonlinear Systems Driven by a Biharmonic Pump. Phys. Rev. Lett. **113**, 247003 (2014).
[29] J. M. Elmirghani, and H. T. Mouftah, All-optical wavelength conversion: Technologies and applications in DWDM networks, IEEE Commun. Mag. **38**, 86 (2000).
[30] S. B. Yoo, Wavelength conversion technologies for WDM network applications, J. Lightwave Technol. **14**, 955 (1996).
[31] Y. Sato, Y. Tanaka, J. Upham, Y. Takahashi, T. Asano, and S. Noda, Strong coupling between distant photonic nanocavities and its dynamic control. Nat. Photon. **6**, 56 (2012).
[32] R. Konoike, H. Nakagawa, M. Nakadai, T. Asano, Y. Tanaka, and S. Noda, On-demand transfer of trapped photons on a chip. Sci. Adv. **2**, e1501690 (2016).
[33] M. Notomi, and S. Mitsugi, Wavelength conversion via dynamic refractive index tuning of a cavity. Phys. Rev. A **73**, 051803 (2006).
[34] K. Kondo, and T. Baba, Dynamic Wavelength Conversion in Copropagating Slow-Light Pulses. Phys. Rev. Lett. **112**, 223904 (2014).
[35] E. J. Reed, M. Soljačić, and J. D. Joannopoulos, Color of Shock Waves in Photonic Crystals. Phys. Rev. Lett. **90**, 203904 (2003).
[36] S. F. Preble, Q. Xu, and M. Lipson, Changing the colour of light in a silicon resonator. Nat. Photon. **1**, 293 (2007).

[37] K. Kondo, and T. Baba, Slow-light-induced Doppler shift in photonic-crystal waveguides. Phys. Rev. A **93**, 011802 (2016).
[38] S. Noda, A. Chutinan, and M. Imada, Trapping and emission of photons by a single defect in a photonic bandgap structure. Nature **407**, 608 (2000).
[39] Y. Akahane, T. Asano, B. S. Song, and S. Noda, High-Q photonic nanocavity in a two-dimensional photonic crystal. Nature **425**, 944 (2003).
[40] B. S. Song, S. Noda, T. Asano, and Y. Akahane, Ultra-high-Q photonic double-heterostructure nanocavity. Nat. Mater. **4**, 207 (2005).
[41] E. Kuramochi, M. Notomi, S. Mitsugi, A. Shinya, T. Tanabe, and T. Watanabe, Ultrahigh-Q photonic crystal nanocavities realized by the local width modulation of a line defect. Appl. Phys. Lett. **88**, 041112 (2006).
[42] H. Ramezani, P. K. Jha, Y. Wang, and X. Zhang, Nonreciprocal Localization of Photons. Phys. Rev. Lett. **120**, 043901 (2018).
[43] R. Konoike, Y. Sato, Y. Tanaka, T. Asano, and S. Noda, Adiabatic transfer scheme of light between strongly coupled photonic crystal nanocavities. Phys. Rev. B **87**, 165138 (2013).
[44] E. Yablonovitch, T. Gmitter, R. Meade, A. Rappe, K. Brommer, and J. D. Joannopoulos, Donor and Acceptor Modes in Photonic Band Structure, Phys. Rev. Lett. **67**, 3380 (1991).
[45] H. Lira, Z. Yu, S. Fan, and M. Lipson, Electrically Driven Nonreciprocity Induced by Interband Photonic Transition on a Silicon Chip, Phys. Rev. Lett. **109**, 033901 (2012).
[46] S. G. Johnson, and J. D. Joannopoulos, Block-iterative frequency-domain methods for Maxwell's equations in a planewave basis. Opt. Express **8**, 173 (2001).
[47] Y. Meyer, and R. Coifman, *Wavelets: Calderón-Zygmund and Multilinear Operators* (Cambridge University Press, Cambridge, 1997), Vol. 48.
[48] I. Daubechies, *Ten Lectures on Wavelets* (Society For Industrial, Philadelphia, 1992).
[49] Y. Xiao, G. P. Agrawal, and D. N. Maywar, Spectral and temporal changes of optical pulses propagating through time-varying linear media, Opt. Lett. **36**, 505 (2011).
[50] See Supplementary Material at http://link.aps.org/supplemental/10.1103/PhysRevApplied.13.044037 for the details of signals and systems theory about the wavelength conversion in the cascaded system.